Journal of Optoelectronic and Biomedical Materials Vol. 17, No. 2, April – June 2025, p. 87 - 97

Bio-logical effect on fungi, bacteria and cancer cells with a study of the aging of selenium dioxide particles produced by pulsed laser

M. A. Yaseen [a,*], A. M. Ali [a], A. N. Abd [b,*]
[a] *Physics Department / College of Education for Pure Science / Tikrit University/ Iraq*
[b] *Physics Department /College of Science / Mustansiriyah University / Baghdad/ Iraq*

There are several ways to produce nanoparticles, but the pulsed laser method with deionized water has been found to be the easiest. All materials change over time and nanoparticles NPs can "age" during storage, and the effect of this may lead to varying results in terms of observed toxicity for nominally the same NPs. The aim of the study was to determine whether (and to what extent) changes in the properties of SeO_2 NPs occur over time. Spherical and clustered selenium dioxide nanoparticles SeO_2 NPs were synthesized using pulsed laser ablation in deionized water, and using a pulsed Nd:YAG laser with an energy of 400 mJ and 200 pulses. The topographic, compositional, morphological and optical properties of SeO_2NPs were studied using AFM, ultraviolet spectroscopy, XRD, SEM, and the optical energy gap of the generated SeO_2 nanoparticles was evaluated using optical properties to measure UV-vis was found to be close to 3.37 Ve. The XRD patterns also show that the as-synthesized SeO_2 NPs are Nano crystals and have face-centered cubic FCC. The prepared solutions were used to inhibit the reproduction of bacteria and fungi *Staphylococcus aurous, Staphylococcus epidermises, Escherichia coli, Klebsiella Pneumoniae and Candida albicans.* respectively. Preliminary results were compared. With the results we obtained after 90 days of producing the solution, it was found that the inhibition decreased to a maximum of 36% for *Staphylococcus* aurous bacteria. The CL-40 colon cancer cell line was used to investigate the toxicity of the produced selenium nanoparticles. Se NPs' IC50 value for CL-40 was found to be 237 μg/mL, and a dose-dependent reduction of cell viability was noted.

(Received April 5, 2025; Accepted May 21, 2025)

Keywords: Pulsed laser, Selenium dioxide nanoparticles, Antimicrobial effect, XRD, Aging, UV-vis, Colon cancer

1. Introduction

The phrase "there's a lot of space down there" is an invitation to enter a new world of physics, "nanotechnology", first introduced by Dr. Richard in 1959. The study of particle science at nanoscale dimensions is of great importance. Nanoparticles have unique properties for all materials, including selenium. Materials down to nano sizes exhibit many distinct thermal, electrical, chemical, electrochemical and bio-logical properties compared to their larger counterparts. Such as increased chemical reactivity or stability, greater surface area to volume, and increased mechanical strength [1, 2]. The inherent properties of nanoparticles, which can be combined with other materials, reveal many applications that facilitate miniaturization (e.g., electronic devices), weight reduction (due to enhanced material efficiency), and/or increased material functionality (e.g., increased toughness, conductivity, and stability). thermal, solubility, friction reduction, selective molecular detection), and in medicine, among others [1, 3, 4]. Nanoparticles of many materials have been synthesized using physical and chemical methods [5, 6]. One of the most environmentally friendly ways to produce NPs is through pulsed laser ablation in liquids (PLAL), which involves laser ablation of metal objects immersed in a liquid medium. The PLAL method involves repeatedly firing laser pulses at an immersed metal target. The atomic

* Corresponding author: ahmed_naji_abd@uomustansiriyah.edu.iq
https://doi.org/10.15251/JOBM.2025.172.87

groups and vapor are discharged into a thick column that rapidly agglomerates the NPs in the medium that is liquid. The NPs produced by PLAL are dispersed uniformly across the aqueous medium. through modifying the aqueous ablation fluid's and the laser's settings [7, 8]. Advances in technology have improved scientists' ability to describe nanoparticles and identify practical uses for them. These days, nanoparticles are present in everything from electronics to renewable energy to kitchenware to aircraft. A sustainable and promising future is possible with nanotechnology [9]. Forty years of sophisticated interaction between science and medical nanotechnology have led to modern nanobiotechnology. Several medical specialties are now using it in novel ways [10]. Selenium (Se), with atomic number 34 and atomic mass 78.96, is an important semiconductor. With an energy gap of 1.74 eV, it has six naturally occurring stable isotopes. According to the American Physical Society and the Materials Research Society, Se is an energy-critical element [11]. One of the most important trace minerals in biology and medicine is selenium. It is found on the formation of selenium proteins with selenocysteine. It is a direct cofactor of oxidoreductase enzymes, including thioredoxin reductase and glutathione peroxidase.[12]. Thus protecting the human body from immune-related disorders. Human understanding of the biogeochemical factors that influence the distribution and transport of environmental selenium has become essential for assessing health concerns related to selenium [13, 14]. The third most prevalent type of cancer in the world is colorectal cancer. Particularly in patients who are advanced in their disease and need rigorous chemotherapy, it starts with the development of polyps that spread, which usually leads to poor response and high rates of morbidity because of multidrug resistance and serious side effects on non-cancerous cells [15]. There are recent developments in the field of targeted nanoparticles against colorectal cancer, and the promising use of ligands and cellular targets in potential strategies in colorectal cancer treatment. Metal compounds that exhibit cytotoxic properties for cancer cells are potential options for chemotherapy. [16, 17]..When materials or compounds undergo physical, chemical, or biological changes over time due to exposure to internal or external influences, this phenomenon is referred to as “chronological aging”. This aging is an important problem in many disciplines, including materials science, medicine, chemistry, and engineering, as it can affect the functional properties or performance of materials [18]. Over time, many properties of NPs change during storage under different conditions, and by “chronological aging” or over time even under optimal conditions [19, 20]. Such temporary changes in the properties of NPs may modify their toxicity, by increasing or decreasing their permeability. The rate of dissolution, or change in agglomeration state, can depend on bioavailability [21, 22]. In this current work, we use a good strategy for producing nanostructured selenium. Here, we demonstrate how Nd:YAG laser ablation of Se produces SeO_2 NPs. The target without the use of any surfactants in D.W [23]. In addition, the effect of time aging on the bio-logical uses of SeO2 NPs was presented and compared with published results.

2. Experimental work

Using the pulsed laser (PLAL) method, selenium dioxide was produced as shown in the following Fig.ure 1. We used pure red selenium, which was first ground and then screened, and the sample was compressed in a 2 cm diameter mold using a 5 ton press machine for 15 minutes. Next, the plankton in the sample was removed with distilled water, and the disc was then placed in a beaker containing deionized water for use. Using a pulsed Nd:YAG laser with an energy of 400 mJ, a frequency of 8 Hz, and a pulse diameter of 2.3 mm. Preparation was carried out using a pulse number of 200. The solution containing nanoparticles was prepared by casting and evaporation method, as shown in Fig.1. Thin films were manufactured. This is done by pouring drops of the solution onto a glass substrate placed on an electric heater at a temperature of 60 degrees Celsius under normal laboratory conditions. We made measurements to analyze structural, topographic and morphological features. The crystal structure and topography of SeO2 NPs were determined by atomic force microscopy (AFM) and X-ray imaging. Using ultraviolet (Uv-vis) measurement, the optical properties were studied. The functional groups from which the SeO2 nanoparticles were made were studied using FTIR analysis. By using agar diffusion, the antibacterial activity of

several species was examined. How to prepare the bacterial suspension: Take a spoonful of sterile normal saline solution and fill the loop with an experimental bacterial isolate. Colloid volume was determined according to McFarland guidelines. Take 100 µL of the suspension onto Mueller-Hinton agar plates for inoculation. Next, we spread it in an L-shape and created holes on the surface of the Mueller-Hinton agar plate. Next, each well was filled with sample solution, and the plates were incubated at 37°C. After 24 h of incubation, the inhibition zone was finally measured.

To study the aging process after (90 days) of sample preparation, we also repeated the inhibition test process in the same way. The inhibition zones were compared between the two cases. Finally, We performed inhibition experiments on colon cancer cells as shown below.

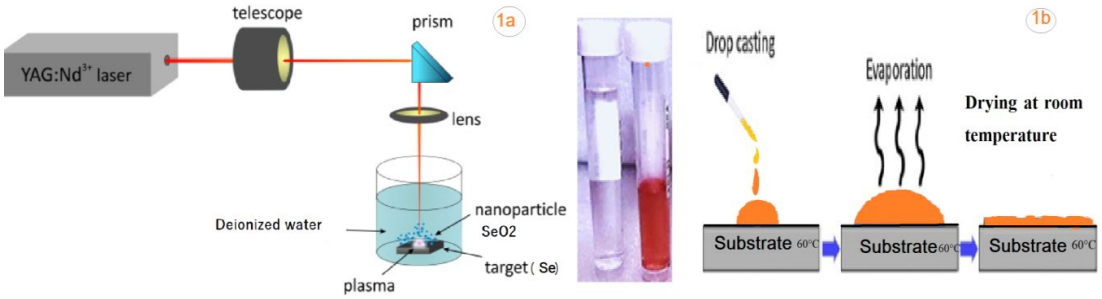

Fig. (1a) Left: Selenium dioxide nanoparticles by pulsed laser method. Middle: color change and formation of selenium oxide nanoparticles. right: Drop casting technique for depositing the solution on the glass substrate(1b).

3. Result and dissection

3.1. Patterns of X- ray diffraction

Using XRD, the crystal structure of SeO_2 NPs was characterized which is usually applied to identify the chemical composition and crystal structure of a specific target. In Fig. 2 the XRD pattern of selenium oxide nanoparticles made using pulsed laser is shown. The crystalline nature of SeO_2 NPs has been confirmed by several investigations, although additional diffraction peaks were detected [24]. The nanocrystalline/amorphous nature of the eye was confirmed by applying XRD, which revealed large diffraction peaks in the microchannels. However, XRD examination of red selenium oxide showed drutin in the full spectrum of 2θ values between 10^0 and 80^0. The diffraction peaks at 2θ values of **23.13** and **29.9**° can be attributed to levels 210 and 211, respectively. These results are consistent with the study [25]. Equation one illustrates how Scherer's formula was used to determine the crystallite size of SeO_2NPs [26].

$$D = \frac{K\lambda}{\beta cos\theta} \tag{1}$$

where k is the shape factor 0.94 in our case, λ is the wavelength of the X-rays, β is the radian of the FWHM, and Θ is the Bragg angle. As a result, the average size of SeO_2-NPs was 38.89nm, which is consistent with the FESEM analysis. Also, the micro stress factor η, the dislocation density δ, and the lattice constant d are calculated. The results we have obtained are shown in Tab 1. From these results, it is clear that it is appropriate to prepare SeO_2 NPs by laser ablation in deionized water. This is due to the formation of plasma, the formation of ions in the aqueous solution.

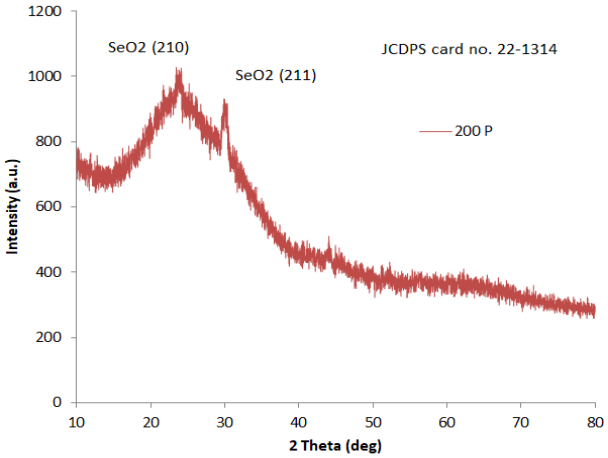

Fig. 2. XRD patterns of thin films of SeO_2 nanoparticles.

Table 1. Parameters for X-RAY characterization of SeO_2 nanoparticles.

Laser pulses	Laser Energy(mJ)	2 θ (deg)	hkl plane	d(A^0)	FWHM(deg)	D(nm)	$\delta*10^{14}$ (lin.m^{-2})	$\eta*10^{-4}$ (lin^{-2}.m^{-4})
200	400	23.13	210	7.642	1.69	4.772	43.903	7.260
		29.9	211	5.939	0.6	13.633	5.380	2.541

4. Scanning electron microscope scene (SEM).

Fig. 3. shows SEM images of the sample generated using 200 pulses of pulsed laser exposure with an energy of 400 mJ confirming that the nanoparticles (SeO_2 NPs) are spherical in shape and size, with a homogeneous concentration and distribution and that at least one of their nanoscopic dimensions is not less than 26.82 nm. The slide contains a few larger, rock-shaped clusters made of small, aggregated particles. There is also dense focus spread across the floor of the model. This indicates that the ablation energy leads to the production of clusters whose size and concentration increase with increasing laser power. The aggregation of these molecules is a characteristic of an aqueous solution, due to the polarization property of water molecules, which leads to the ions combining with each other and re-forming large aggregates. These results are consistent with the study [27].

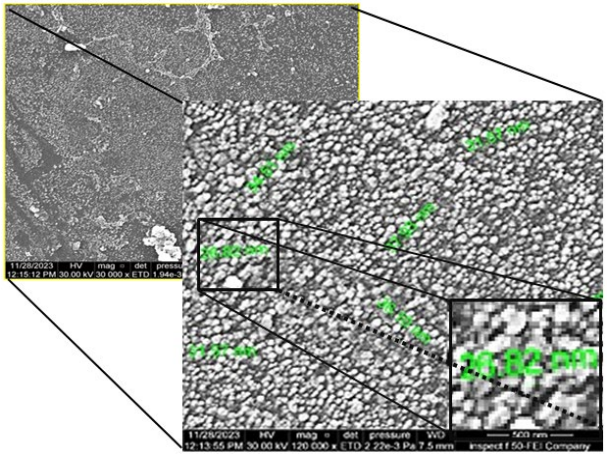

Fig. 3. FE-SEM image of selenium dioxide nanoparticles.

5. Atomic force microscopy (AFM)

We use atomic force microscopy (AFM) as a means of analyzing the surface topography of thin films to obtain microscopic details regarding the surface structure of thin films. This technique provides topographical representations that accurately describe the surface topography. Fig. 4. shows the 3D AFM images and accumulation distribution diagram of the prepared nanoparticles (SeO2:NPs), which were produced using a pulsed laser in a solution of deionized water, and then deposited on a glass substrate under laboratory conditions at a temperature of 60 °C. It is clear that the particles are almost spherical in shape and are well and homogeneously distributed on the substrate. The grains appear homogeneous and vertically aligned. Using special software, their average size was estimated to be approximately 150 nm, while the root mean square (RMS) values of roughness were estimated to be approximately 1.51 nm and 27.05 nm, respectively. Tab 2. shows this the large differences in the average and root values of roughness can infer the regularity and homogeneity of the surface.

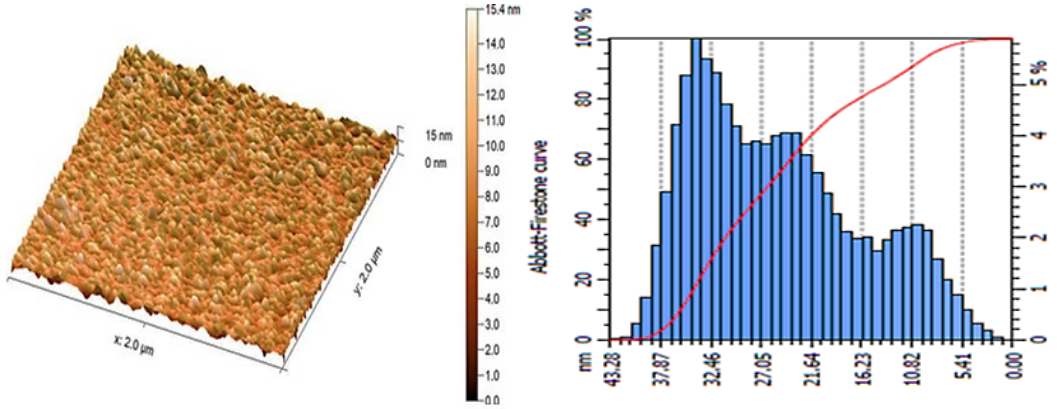

Fig. 4. 3D AFM image and Granularity accumulation distribution chart of SeO_2 nanoparticles.

Table 2. The Average value, roughness average, and Root mean square.

Samples	Average value (nm)	Roughness average (nm)	Root mean square (nm)
200 P	15	27.05	1.51

6. FTIR measurement results

The absorption spectrum represents the vibrational energy levels of each bond, and has specific values for the energy of the absorbed photons. The dried sample of SeO_2 NPs was subjected to Fourier transform infrared (FTIR) spectra using a Shimadzu 8400 FTIR spectrophotometer in the waveband of 400 - 4000 1/cm with a resolution of 41/cm. The type of effective chemical bonds in all phases of molecular compounds was determined, and in Fig. 5. the functional groups were identified as follows: first at the wave number 3436 cm^{-1} , which is due to the hydroxide bond O-H stretching of water [28]. The investigation indicates that the second peak is at wave number 2350cm^{-1}, or O-C-O stretching. This is found for all models, due to the environmental conditions of the experiment, which worked in an open place exposed to atmospheric air. As for the bottom of the transmittance curve at the wave number 1637 cm^{-1}, it goes back to the water molecule H-O-H bending water, which represents the medium in which the work is produced, as the study has represented in the reference agrees. As for the absorption spectrum at the wavenumber 512 cm^{-1}, it refers to the two models [29]. which represent the original work prepared by the pulsed laser method for a sample of the red element selenium, which produced selenium dioxide O-Se-O bending, as shown in Tab 3.

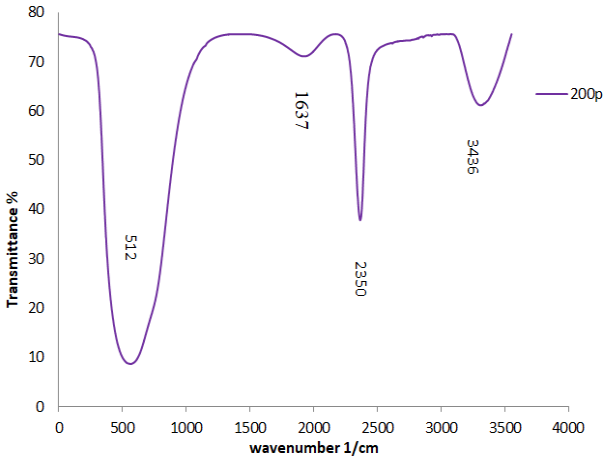

Fig. 5. FTIR spectra of SeO_2 NP_S samples with laser Pulses(200P).

Table 3. Chemical bonds and infrared resonance sites for SeO_2:NPs.

No .of Pulses	Energy pules(mJ)	Bands assignments	O-H stretching of water	O-C–O stretching	H-O-H bending water	0-Se-0 bending
100P	400	Wavenumber(cm^{-1})	3436	2350	1637	512

7. Optical properties

Using UV-Vis spectroscopy, the absorption range as a function of the wavelength of electromagnetic radiation 200-1100 nm, as in Fig. 6. The absorbance of the SeO_2 aqueous solution, reveals three regions of UV absorption. Absorption decreases sharply due to the expansion of the size of absorbed molecules. Because the incident photons have sufficient energy. To excite electrons from the valence band to the conduction band. In the wavelength region (visible light), the absorbance of the film decreases with increasing length. Because photons do not have enough energy to interact with atoms. Fig. 6 shows the energy gap of selenium dioxide. The straight part of the graph near the absorption edge is extended until it meets the photon energy axis in order to determine the size of the energy gap. It was found that the energy gap values of the manufactured material (SeO_2 NPs) increased from 1.72 eV in its bulk state to 3.65 eV for the model that was created, with a difference of 1.93 eV.

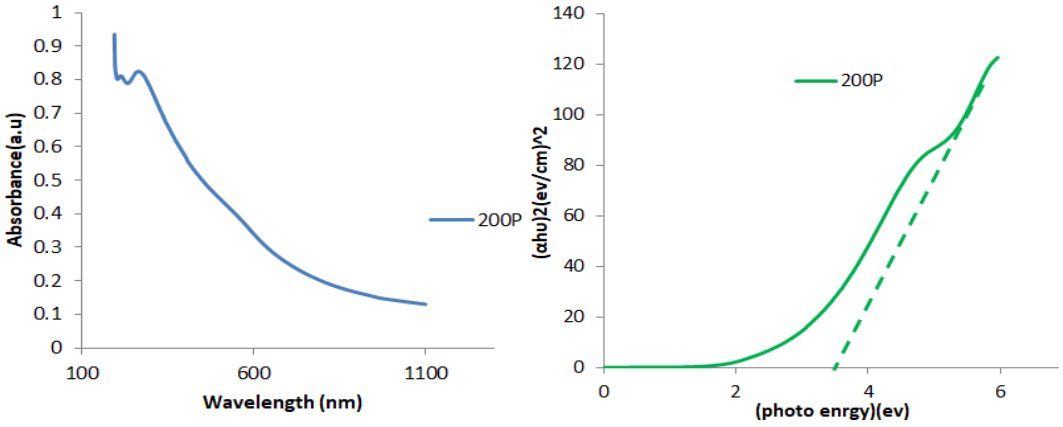

Fig. 6. The sample's (SeO_2NPs) absorption of UV –Vis wavelengths, and the gap energy calculation.

8. Antimicrobial activity

Using well diffusion technique, the antibacterial activity of the prepared nanoparticles, SeO_2 NPs, prepared in deionized water solution was investigated by pulsed laser method. The bacteria were *S. aurous, S. epidermises, E. coli and K. Pneumonia* is one of the most important species. Dangerous bacteria that this technology was used to combat. In addition to one species of *C. albican* fungus. It is clear from the results that we obtained during the first stages mentioned in Table 5, and shown in Fig. 7, that the prepared compounds have a great ability to prevent bacterial growth to varying degrees depending on the type of bacteria. A comparison was also made in this study with the inhibition test for the prepared material (selenium dioxide nanoparticles) by testing the time factor (for time aging). The testing process was repeated 90 days after the substance was prepared in the laboratory, and the results showed that the inhibition process or the effect of the substance became much less than it was when the substance was fresh Shown in the diagram 1. These results may be due to changes in the size of SeO_2 particles, increased agglomeration over time, or it may also be due to a decrease in the concentrations of the particles of the substance due to the adhesion of nanoparticles to the walls of the container over time [30].The inhibition mechanism of the substance has been explained in several ways, including: The tendency of nanoparticles to discharge metal ions is likely the reason behind their strong antibacterial effect[31]. Or the chemical composition, tendency to release metal ions causing electron transfer across the membrane, and oxidation upon penetration of cell components are responsible for the significant antibacterial activity of nanoparticles. Or excessive production of reactive oxygen species (ROS) causes “oxidative distress” or molecular damage to the cell[32] . The antifungal and antibacterial effect of nanoparticles can be attributed to the interaction of SeO_2NPs with the outer membrane of fungi as a result of the increase in their surface area ratio, which leads to the cessation of respiration and some other metabolic pathways, which in turn leads to impaired transport and impaired respiration. Or interruption of energy transfer, leading to cell death.

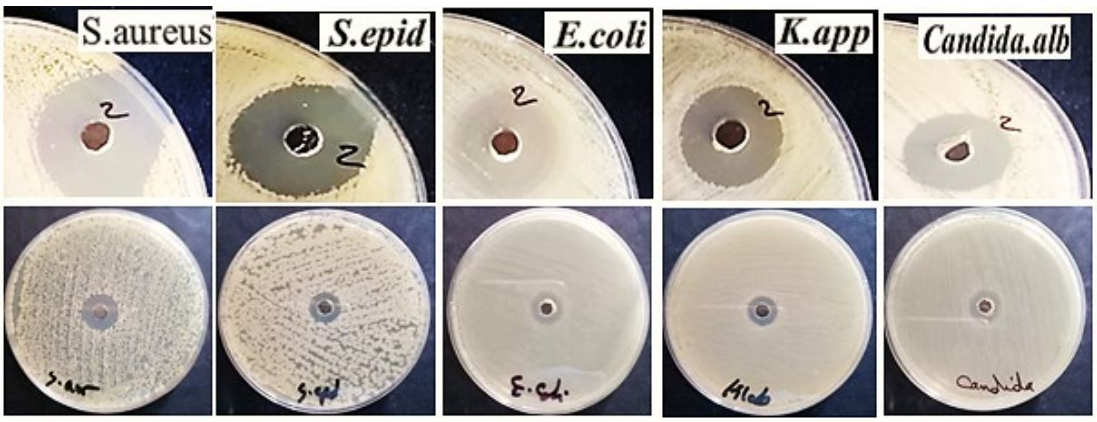

Fig. 7. Areas of inhibition of bacterial and fungal isolates by selenium dioxide nanoparticles produced using a pulsed laser for 200 pulses, The top picture is within 24 hours of producing the compound. The bottom picture is 90 days after the material was produced

Table 4. Shows the bacteria and fungi inhibition diameter of selenium dioxide produced by pulsed laser 200P.

Bacteria and fungus	Longevity	S. aureus	S. epidermises	E. coli	K. Pneumoniae	C. albicans
Inhibition zone (mm) of SeO_3 NPs	Fresh	25	22	17	20	19
	After 90 days	16	14	14	14	15

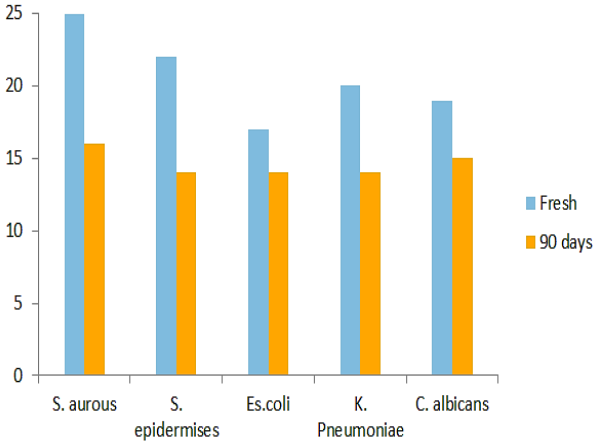

Diagram 1. A diagram showing the diameter of the inhibition zone per bacterium for a solution of selenium dioxide produced using a pulsed laser 200P.

9. Biomedical tests

CL-40 Cell line: The primary colorectal cancer (TNM stage 3) in a woman's right colon gave rise to human (Homo sapiens) colon carcinoma; the literature noted that the cells were well differentiated. The cell line had progressed to the point where it could form monolayers at 37°C in a humidified atmosphere with 5% CO2. During the assays, the cell line was maintained in serum-free DMEM/HAM-F12 conditions. The tests showed that cells were cultured in the medium at various intervals. Aluminum foil protected the cells from the light. One day after the cells were sown, RA and DMSO were added to prevent any interactions with cell adherence to the culture dishes. In all experiments, tumor cells were cultivated to approximately 90% confluence before being separated into single-cell suspensions from tissue culture flasks using 0.05 percent EDTA in PBS for three minutes.

9.1. MTT assay

The cells (1 x 10^4 to 1 x 10^6 cells mL^{-1}) were cultivated in 96-well plates until each well held 200 mL of full culture medium. Sterile Parafilm was placed over the plates, which were then gently swirled and incubated for 24 hours at 37 °C with 5% CO2. 200 µl of a two-fold serial dilution of materials NPs solutions (25 µg/mL) was added to the wells after the medium was removed following incubation. Three duplicates of the concentration and control tests were conducted. For 24, 48, and 72 hours, the plates were incubated at 37°C with 5% CO2. Following the extract exposure, 10 mL of MTT solution was added to each well. The plates were then incubated with 5% CO2 for a further four hours at 37°C. The medium was carefully removed, and 100 mL of DMSO solubilization solution was added to each well. The wells were then incubated for five minutes. An ELISA reader (Bio-rad, Germany) was used to measure the absorbance at a wavelength of 575 nm. The percentage of cell viability was expressed using the untreated cells

control (100% cell viability). The optical density results were statistically analyzed to get the IC50. This problem can be resolved using the following equation:

$$Viability(\%) = \frac{optical\ density\ of\ sample}{optical\ density\ of\ control} \times 100\% \quad (2)$$

The CL-40 cell line, which has 1x105 ml-1 cells per well in its exponential development phase, was utilized to test the cytotoxicity of produced Se NPs. For a full day, they were incubated with increasing concentrations of Se NPs. The MTT assay was used to examine the cell viability, which was expressed as a percentage of the untreated control (100 percent cell vitality). Figure 8 displays the cytotoxicity results of CL-40 cell viability following a 24-hour treatment with different doses of Se NPs. Se NPs solutions led to a significant drop in the survival rate of CL-40 cells in dosage dependency ($P<0.0001$), and all results showed a concentration-dependent decrease in cell viability. There are substantial changes for colon CL-40 carcinoma at values between 400 and 1000 µg/mL, but not at concentrations below 100 µg/mL. The IC50 for the cytotoxicity action was 273 µg/mL.

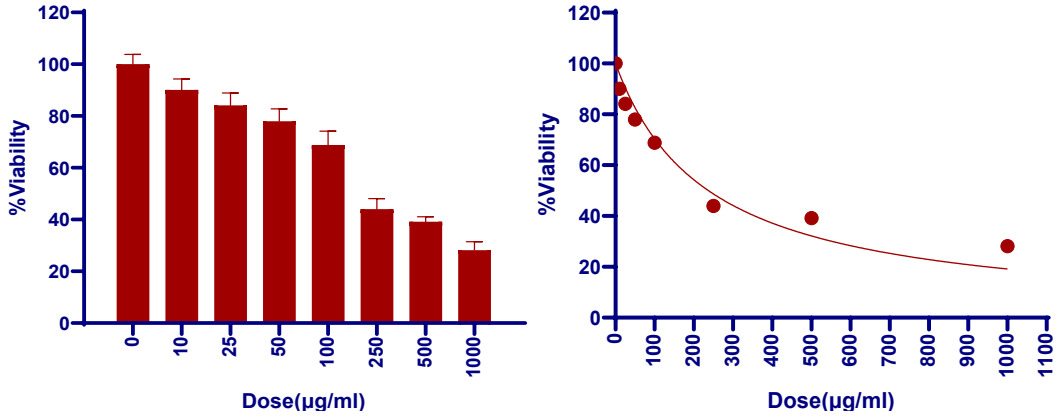

Fig. 8. Cell viability rate of syntheses Se NPs at concentrations of (0-1000) µg/mL with CL-40 cell.

The cytotoxicity results of synthesized Se NPs against CL-40 are shown in Figure. (8) and Table (5). Cell viability loss was observed, which was dose-dependent and the determined IC50 value of Se NPs for CL-40 was (237 µg/mL).

Table 5. Cell viability (mean ± standard deviation (SD) of syntheses Se NPs treatment on CL-40 cell line.

Dose(µg/ml)	Mean	SD	N
0	100	3.762855305	3
10	90.07238883	4.247477307	3
25	84.10892796	4.775304545	3
50	77.93864185	4.819885918	3
100	68.83833161	5.307730819	3
250	43.98483282	4.084907429	3
500	39.19338159	1.870024956	3
1000	28.12823164	3.284876975	3

10. Conclusion

The present work has shown that to produce SeO_2NPs using the pulsed laser (PLAL) method, it is possible to obtain Nano scale sizes. From the analysis, XRD and SEM investigations revealed that the nanoparticles are face-centered cubic (FCC). SEM revealed an agglomeration of spherical particles with a minimum diameter of 26 nm. In the bio-logical application, it was found that the diameter of inhibition decreased for the fungus C. albicans from 19 to 15 mm, and the highest rate for the bacteria E. coli from 17 to 14 mm, after 90 days of production. The difference in effect (inhibition) depends on the concentrations and shapes of the molecules and the type of bacteria. An increase in the number of molecules leads to an increase in the process of incorporation of selenium oxide nanoparticles with the DNA bases of pathogenic bacteria and the formation of cross-links that replace hydrogen bonds between purines and pyrimidines adjacent to the nitrogen. Cell death will result from the DNA shrinking, losing its structure, and being unable to replicate. Our knowledge of the biological characteristics of nanoparticles has improved in recent years. The use of bio-based applications to treat colorectal cancer shows potential. Relevant requirements include clearance via glomerular filtration in the kidneys (between 10 and 100 nm) and an ideal size to prevent an immunological response [33]. A spherical form is ideal for extending circulation time and accelerating cancer cell uptake [16]. Enough targeting ligands (range: 0.5–5%) on the surface of nanoparticles to enhance tissue-specific targeting [34].

References

[1] Abd Al Hussan, S.M., N.A. Bakr, A.N. Abd, IOP Conference Series: Materials Science and Engineering. 2020. IOP Publishing; https://doi.org/10.1088/1757-899X/928/7/072142

[2] Haleem, A., et al., Global Health Journal, 2023. 7(2): p. 70-77; https://doi.org/10.1016/j.glohj.2023.02.008

[3] Mezher, T.A., A.M. Ali, A.N. Abd, International Journal of Nanoscience, 2023. 22(04): p. 2350026; https://doi.org/10.1142/S0219581X23500266

[4] Fazio, E., et al., Nanomaterials, 2020. 10(11): p. 2317; https://doi.org/10.3390/nano10112317

[5] Noori, A.J., I.M. Ali, Journal of Optics, 2024: p. 1-8; https://doi.org/10.1007/s12596-024-02210-4

[6] Jondle, C.N., et al., PLoS pathogens, 2018. 14(10): p. e1007338; https://doi.org/10.1371/journal.ppat.1007338

[7] Amendola, V., M. Meneghetti, Physical Chemistry Chemical Physics, 2013. 15(9): p. 3027-3046; https://doi.org/10.1039/C2CP42895D

[8] Anastas, P., N. Eghbali, Green chemistry: principles and practice. Chemical Society Reviews, 2010. 39(1): p. 301-312; https://doi.org/10.1039/B918763B

[9] Kalidasan, B., et al., Renewable Energy, 2021. 173: p. 1057-1069; https://doi.org/10.1016/j.renene.2021.04.050

[10] Malik, S., Y. Waheed, Dentistry Journal, 2023. 11(11): p. 266; https://doi.org/10.3390/dj11110266

[11] Rahman, A., Synthesis of Selenium Nanostructures: Rods, Wires, and Fibers by Pulsed Laser Ablation in Liquids. 2024, University of Arkansas at Little Rock; https://doi.org/10.1016/j.matlet.2024.137476

[12] Shareef, B.Q., H.I. Al Qadhi, A.J. Shayma'a, Journal of the Faculty of Medicine Baghdad, 2024. 66(1): p. 58-66; https://doi.org/10.32007/jfacmedbagdad.6612174

[13] Zhang, T., et al., Frontiers in nutrition, 2023. 10: p. 1183487; https://doi.org/10.3389/fnut.2023.1183487

[14] Fordyce, F., Ambio, 2007: p. 94-97; https://doi.org/10.1579/0044-7447(2007)36[94:SGAH]2.0.CO;2

[15] Tiwari, A., et al., Drug delivery and translational research, 2020. 10(2): p. 319-338;

https://doi.org/10.1007/s13346-019-00680-9
[16] Cisterna, B.A., et al., Nanomedicine, 2016. 11(18): p. 2443-2456; https://doi.org/10.2217/nnm-2016-0194
[17] Farinha, P., et al., Drug delivery and translational research, 2022: p. 1-18; https://doi.org/10.1007/s13346-021-00916-7
[18] Mitrano, D.M., et al., Environment international, 2015. 77: p. 132-147; https://doi.org/10.1016/j.envint.2015.01.013
[19] Badawy, A.M.E., et al., Environmental science & technology, 2010. 44(4): p. 1260-1266; https://doi.org/10.1021/es902240k
[20] Tejamaya, M., et al., Environmental science & technology, 2012. 46(13): p. 7011-7017; https://doi.org/10.1021/es2038596
[21] Jacobson, A.R., et al., Environmental pollution, 2005. 135(1): p. 1-9; https://doi.org/10.1016/j.envpol.2004.10.017
[22] Pal, S.K., et al., Materials Science and Engineering: B, 2020. 259: p. 114598; https://doi.org/10.1016/j.mseb.2020.114598
[23] Jadhav, A.A., P.K. Khanna, RSC Advances, 2015. 5(56): p. 44756-44763; https://doi.org/10.1039/C5RA05701A
[24] Srivastava, N., M. Mukhopadhyay, Powder technology, 2013. 244: p. 26-29; https://doi.org/10.1016/j.powtec.2013.03.050
[25] Bukalo, N.N., et al., Open Geosciences, 2017. 9(1): p. 407-418; https://doi.org/10.1515/geo-2017-0031
[26] Mezher, T.A., A.M. Ali, A.N. Abd, International Journal of Nanoscience, 2023. 22(04): p. 2350035; https://doi.org/10.1142/S0219581X23500357
[27] Yuwono, V.M., et al., Faraday Discussions, 2012. 159(1): p. 235-245; https://doi.org/10.1039/c2fd20115a
[28] Abd, A.N., Improved photoresponse of porous silicon photodetectors by embedding CdS nanoparticles. World Scientific News, 2015. 19: p. 32-49.
[29] Izzo, F., et al., Infrared Physics & Technology, 2020. 106: p. 103266; https://doi.org/10.1016/j.infrared.2020.103266
[30] Pinto, V.V., et al., Colloids and Surfaces A: Physicochemical and Engineering Aspects, 2010. 364(1-3): p. 19-25; https://doi.org/10.1016/j.colsurfa.2010.04.015
[31] Alwan, B.J., A.N. Abd, N.H. Zaki, AIP Conference Proceedings. 2023. AIP Publishing; https://doi.org/10.1063/5.0176320
[32] Ajaj, K., M.A. Al-Jubbori, A.M. Ali, Nanosistemi, Nanomateriali, Nanotehnologii, 2024. 22(3).
[33] Woynarowski, J.M., et al., Molecular pharmacology, 1998. 54(5): p. 770-777; https://doi.org/10.1124/mol.54.5.770
[34] Hrkach, J., et al., Science translational medicine, 2012. 4(128): p. 128ra39-128ra39; https://doi.org/10.1126/scitranslmed.3003651